Experimental Characterization of Hybrid Supercapacitor Under Different Operating Conditions Using EIS Measurements

Marcantonio Catelani, *Member, IEEE*, Lorenzo Ciani, *Senior Member, IEEE*, Fabio Corti, *Member, IEEE*, Maurizio Laschi, Gabriele Patrizi, *Member, IEEE*, Alberto Reatti, *Member, IEEE*, and Dario Vangi

***Abstract*— Hybrid supercapacitors (HSCs) are innovative energy storage solutions that are becoming essential in many fields of applications. Their performances are strongly influenced by several parameters, such as temperature conditions, load characteristics, and state-of-charge (SOC). For this reason, it is becoming fundamental to characterize their performances under different scenarios. One of the best ways to investigate the performances is by employing the electrochemical impedance spectroscopy (EIS) measurement. However, since HSC is a recent technology, databases and studies focused on impedance analysis are not currently available in the literature. For this reason, this work presents the results of a large measurement campaign carried out to acquire impedance data on a large frequency range (from 1 mHz to 100 kHz) under different temperatures and SOC conditions. The constructed dataset has been used to investigate impedance anomalies and to analyze the effects that temperatures and SOC may have on the HSC impedance. The large obtained dataset can also be used for diagnostic and prognostic purposes. The dataset used in this study is available at https://doi.org/10.6084/m9.figshare.24321496.**

***Index Terms*— Dataset, electrochemical impedance spectroscopy (EIS), impedance measurement, prognostics and health management, supercapacitors (SCS), testing.**

I. Introduction

ENERGY storage plays a vital role in meeting the growing global demand for reliable and sustainable energy solutions. Among various electrochemical energy storage (EES) technologies, supercapacitors (SCs) have emerged as a promising alternative to conventional batteries due to their unique advantages [1]. Due to their high power density, SCs (also known as ultracapacitors) offer significant advantages over traditional batteries in several key areas. This technology can quickly store and release energy, making it ideal for applications such as regenerative braking in electric vehicles or smoothing out power fluctuations in renewable energy systems [2]. Another advantage is exceptional cycle life. Unlike batteries, which suffer from limited charge-discharge cycles [3], [4], SCs can endure millions of charge–discharge cycles without significant loss in performance [5]. This longevity makes them highly reliable and cost-effective. Furthermore, SCs excel in providing high efficiency during the charging and discharging processes [6]. This efficiency, combined with their ability to handle high currents, makes SCs a valuable asset in applications that require fast response times, such as grid stabilization [7], energy management of hybrid vehicles [8], and peak load shaving [9].

There are several types of SC technologies, based on the type of charge mechanism, detailed in the following.

1) *Electrochemical Double-Layer Capacitors (EDLCs) [10], [11]:* The most common type of SCs. They store energy through the physical separation of charge at the electrode–electrolyte interface. EDLCs typically use high surface area carbon materials as electrodes and an electrolyte solution, which could be either aqueous, ionic, or organic [12]. They offer high power density, fast charge/discharge rates, and long cycle life. On the other hand, they have high auto discharge and a limited shelf life [13], [14].
2) *Pseudocapacitors [15], [16]:* They store energy by electron charge transfer between the electrode and the electrolyte, involving electrosorption or fast redox reactions, and they offer higher energy density compared to EDLCs. Due to the rare materials used, such as ruthenium, the cost of these capacitors is high [17].
3) *Hybrid SCs (HSCs) [18], [19]:* Combine two different types of storage of charge. This involves sharing the features of EDLCs, pseudocapacitors, and/or batteries. There are two main types of HSCs depending on the internal structure.
    a) Internal serial hybrid is an asymmetric electrochemical capacitor with one electric double-layer capacitor and another battery-type electrode, such as Superbatteries.[1]
    b) Internal parallel hybrids, SCs, and battery materials are mixed to form bimaterial-type electrodes, such as Ultrabatteries.[1]

One of the most promising combines an EDLC electrode and a battery-type electrode, allowing for both high

Manuscript received 28 July 2023; revised 27 September 2023; accepted 17 October 2023. Date of publication 1 November 2023; date of current version 28 December 2023. The Associate Editor coordinating the review process was Dr. Qiang Miao. *(Corresponding author: Lorenzo Ciani.)*

Marcantonio Catelani, Lorenzo Ciani, Fabio Corti, Gabriele Patrizi, and Alberto Reatti are with the Department of Information Engineering, University of Florence, 50139 Florence, Italy (e-mail: marcantonio.catelani@unifi.it; lorenzo.ciani@unifi.it; fabio.corti@unifi.it; gabriele.patrizi@unifi.it; alberto.reatti@unifi.it).

Maurizio Laschi and Dario Vangi are with the Department of Industrial Engineering, University of Florence, 50139 Florence, Italy (e-mail: maurizio.laschi@unifi.it; dario.vangi@unifi.it).

Digital Object Identifier 10.1109/TIM.2023.3329094

[1]Registered trademark.

TABLE I
REVIEW OF THE STATE-OF-THE-ART REGARDING EIS MEASUREMENT FOR SCS

REF.	CELL TECHNOLOGY	NOMINAL PARAMETERS	FREQUENCY	OPERATING CONDITIONS	TEMPERATURE CONDITIONS
[28]	EDLC	1400 F 2.5 V	120 mHz ÷ 70 Hz	[0.6; 1.2; 1.8; 2.4] V	[-30; -10; 5; 20; 35; 50] °C
[32]	EDLC	1400 F 2.5 V	2.1 mHz ÷ 6 kHz	[30; 50; 80; 100] SOC	Room Temperature
[33]	EDLC	350 F 2.7 V	10mHz ÷ 100 Hz	A single unknown condition	[25; 85; 95; 105] °C
[34]	EDLC	350 F 2.7 V	Not specified	2.8 V	[55; 60; 65; 70] °C
[35]	EDLC	25 F 2.7 V	100 mHz ÷ 10 kHz	A single unknown condition	85 °C
[36]	EDLC	1500 F 2.7 V	10 mHz ÷ 100 kHz	2.7 V	65 °C
[37]	EDLC	2000 F 2.7 V	10 mHz ÷ 10 kHz	A single unknown condition	Room Temperature
[38]	EDLC	2600 F 2.7 V	10 mHz ÷ 1 kHz	Different values from 0 V to 2.7 V	25 °C
[39]	EDLC	2600 F 2.5 V	10 mHz ÷ 10 kHz	2 V	25 °C
[40]	EDLC	10 F 2.7 V	1Hz ÷ 5 kHz	A single unknown condition	[0; 25; 50; 75] °C
[41]	Not specified	3000 F 2.7 V	10 mHz ÷ 1 kHz	Different Current Ripple Rate values	[-20; -10; 0; 10; 20; 30; 40] °C
[42]	Not specified	2600 F 2.5 V	10 mHz ÷ 1 kHz	A single unknown condition	25 °C

power density, increased energy density, and high cycle life. HSCs offer a balance between the long cycle life of EDLC electrodes and the higher energy storage capacity of batteries. The downside is the higher cost compared with more industrialized technologies such as lithium-ion (Li-Ion) batteries.

An effective and useful technique to characterize the electrical behavior over a specified range of frequencies of an energy storage cell (e.g., a battery, a fuel cell, or an SC) is electrochemical impedance spectroscopy (EIS) [20]. The impedance of an energy storage cell is composed of two main components: resistance (R) and reactance (X). Resistance represents the loss of energy, while reactance reflects the energy storage and exchange processes, including the capacitive and inductive effects [21]. Thus, EIS measurements represent a valuable tool for monitoring the performance and health of an EES over time [22]. Changes in the impedance spectra may indicate aging, degradation, fluctuation of the operating conditions, or other issues related to the device. By measuring impedance at different operating conditions and comparing the results, it becomes possible to assess the stability, cycle life, and long-term behavior of SCs. This information is crucial for developing strategies to mitigate degradation and enhance the durability of these energy storage devices. Recent literature is paying significant attention to EIS measurement across several fields of application, including batteries [23], [24], fuel cells [25], [26], advanced biosensing applications [27], and SCs [28]. However, while EIS investigation of Li-Ion batteries is a widely discussed topic, there are only a few papers dealing with SC characterization through EIS measurements. More importantly, almost all of them deal with EDLC technology, while analyses of HSCs using EIS are currently not available. For instance, the relationship between temperature and impedance of EDLC has been first studied in [29] emphasizing an increase of the equivalent series resistance (ESR) when temperature decreases. This aspect has been further confirmed and expanded in [30] that such dependence is more noticeable at low frequencies. Furthermore, Xiong et al. [31] showed that such dependence is approximately exponential, while the impact of SOC in their experiments is less dominant. However, most of the considerations regarding temperature and SOC dependencies consider only the ESR instead of the entire frequency spectrum of the SC impedance.

A detailed review of the literature has been reported in Table I, emphasizing the cell technology, the frequency range of investigation, the operating conditions in terms of state-of-charge (SOC) or the voltage at which the test has been performed, and the temperature conditions. As can be seen from the table, most of the works performed EIS considering only a limited frequency range of investigation. Furthermore, there is only one work [32] that investigates the performances under different SOCs, but the analysis is carried out only a room temperature. Quite the contrary, the few papers that carried out EIS under different temperature conditions usually performed the measurements considering limited operating conditions (in terms of SOC or voltage condition).

Another fundamental flaw that must be taken into consideration is that all the available papers do not provide the EIS dataset. Currently, to the author's knowledge, there are no publicly available datasets, including EIS measurement of hybrid SCs under several different operating conditions.

Therefore, trying to fill this gap, this article introduces a customized test plan and experimental setup to characterize the performances of HSCs by employing EIS measurement and considering.

1) A large frequency range from 1 mHz to 100 kHz with ten data points per decade.
2) Six different operating conditions in terms of SOC, namely, 0%, 20%, 40%, 60%, 80%, and 100%.
3) Eight different operating temperatures, starting from −20 °C up to 50 °C.

The data acquired during the measurement campaign have then been used to investigate the SC's behavior-changing SOC and operating temperature. In summary, the main contribution of this article is the development of a large EIS dataset for HSCs investigating frequency ranges, temperature conditions, and SOC conditions that are currently not available in the literature. The proposed experimental test allowed the introduction of adequate parameters for the HSCs, as well as the study and discovery of impedance variations and impedance anomalies under different operating conditions that are currently not fully studied and described in recent literature.

II. Device Under Test

An SC whose nominal capacity is 4000 F and maximum voltage is 4.2 V has been chosen for the tests presented in this work. In particular, an internal series HSC, whose cathode is that of a Li-Ion battery and the anode is that of an EDLC, has been used. The device under test (DUT) is commonly identified using the notation 4.2V4000F rechargeable nanopouch capacitor and it is produced by Gonghe Electronics Company Ltd. [43].

In the specific HSC, floccules of reduced graphene oxide (rGO) are dissolved in the electrolyte [44]. Indeed, rGO can increase the ionic conductivity of the electrolyte, improve the thermal and mechanical stability of the membrane, and provide a favorable interface between the electrolyte and the electrode. They have very similar electrical characteristics to Li-Ion batteries, such as the operating voltages or specific energy (∼200 Wh/kg), but unlike them are less susceptible to thermal runaway when misused or shorted. According to the datasheet [43], the maximum continuous charge/discharge current is 5 A, while the maximum peak charge/discharge current is 10 A. Considering standard conditions, the charge limit voltage is 4.2 V, the charge cutoff current is 1 A, and the discharge cutoff voltage is 3 V. Regarding the operating condition, the device can be charged/discharged in the temperature range $[-20, +55]$ °C. They are cylindrical cells with a weight of (70 ± 10) g and pole terminations coming out of the bottom face of the cylinder. The length of the cylinder is (69 ± 2) mm, while the diameter is (24 ± 1) mm. Furthermore, according to the datasheet, the nominal internal resistance values measured at 1 kHz are lower than 15 mΩ. However, it is important to mention that test specifications (in terms of operating temperature and SOC) for the internal resistance measurement have not been specified.

III. Proposed Approach for Dataset Construction

This section illustrates the approach that has been used to construct the dataset for the characterization of HSCs under different temperature and SOC conditions.

A. Testing Procedure

The dataset developed in this work for HSCs characterization is based on two variables that are perturbated during the test to investigate different operating conditions that are typical of several different application fields.

More in detail, six different states of charge have been considered, namely

$$\text{SOC} \in [100\%; 80\%; 60\%; 40\%; 20\%; 0\%].$$

To ensure data consistency, the first step of the procedure requires identifying the actual capacity of the HSC.

More in detail, the SC under test has a nominal capacity of 4 Ah. However, to have a clear and precise determination of the actual SOC, it is necessary to measure the initial capacity of the device before the tests. This is essential because, if the SOC is calculated using the nominal value, there will be slightly inaccurate results. To determine the actual capacity, it is necessary to fully discharge and fully charge the cell consecutively using a constant-current–constant-voltage profile. The current used during the charge and discharge phases of this cycle must be low concerning the nominal capacity of the cell. This is essential to allow a nonstressful charge/discharge condition and to ensure a complete charge profile (in terms of energy stored) and discharge profile (in terms of energy released). Such operation has been performed in the specific HSC using a 0.2 C-rate profile (i.e., 800-mA constant current) and it pointed out an actual capacity value of $C_{\text{act}} = 3.95$ Ah. Finally, using this value, it is possible to determine a certain SOC percentage simply as the specific percentage of C_{act} (e.g., SOC = 20% is obtained as $C_{\text{act}} \cdot 0.2$).

This procedure permits a precise measure of the actual energy stored during the charge and the actual energy released during the discharge phase, thus obtaining exact information regarding the actual capacity value of the device.

Furthermore, eight different temperature conditions have been considered in the proposed experiments, namely

$$\text{Temp} \in [-20; -10; 0; 10; 20; 30; 40; 50]\ ^\circ\text{C}.$$

The EIS measurements have been repeated starting from a fully charged SC (i.e., SOC = 100%) and then discharging the cell until all SOC conditions have been tested. For every defined SOC, EIS measurements have been repeated at all eight temperature values, starting from the coldest temperature up to the hottest value.

After that, all temperature conditions have been investigated for a determined SOC and the cell temperature has been brought back to ambient value. When ambient temperature stability has been ensured, the SC has been fully charged. After 1-h rest time, the cell has been partially discharged until it meets the specified SOC conditions and then repeats all EIS measurements at all considered temperatures.

TABLE II
DETAILED WORKFLOW OF THE TESTING PROCEDURE FOR CHARACTERIZATION OF SCS

Workflow of the testing procedure
Input: $Temp$ = Selected operating temperatures value SOC = State-of-Charge at which EIS is performed
Start
1. Set $Temp = 25\,°C$
2. Charge/discharge cycle using low current for SOC definition
3. Charge the battery up to $SOC = 100\%$
4. $\forall\ SOC \in [100\%;\ 80\%;\ 60\%;\ 40\%;\ 20\%;\ 0\%]$ **do**
5. Set $Temp = -20\,°C$
6. $\forall\ Temp \in [-20;\ -10;\ 0;\ 10;\ 20;\ 30;\ 40;\ 50]°C$ **do**
7. EIS Measurement at a certain SOC and $Temp$
8. Move to the next $Temp$
9. **Repeat** until all $Temp$ are done
10. Set $Temp = 25\,°C$
11. Charge the battery up to $SOC = 100\%$
12. 1 h rest time
13. Discharge the battery until next SOC has been reached
14. **Repeat** until all SOC are done
End
Output: Complete EIS dataset under different SOC and $Temp$

A summary of this cycling testing procedure is reported in Table II, showing all required steps to obtain the full dataset.

It is important to point out that all charging/discharging operations of the cell have been performed at ambient temperature to ensure both safety requirements and consistent results. Furthermore, the tests have been repeated changing all temperature conditions for a specific SOC and then repeating the procedure for a different SOC value (and not vice versa) to ensure that all measurements taken with a defined SOC are obtained in the same operating conditions. Quite the contrary, consistency of temperature conditions is ensured by utilizing a calibrated PT100 resistance temperature detector (RTD) as illustrated in Section III-B.

Looking more in detail at the characteristics of the EIS measurements, for every working condition, EIS has been run in a potentiostatic way within the frequency range from 1 mHz and 100 kHz. The specific frequencies of investigation are distributed on a logarithmic scale, with ten data points for each frequency decade, leading to 81 impedance values for every working condition. Finally, the signal used for the cell excitation is a 5-mV rms sinusoid without dc offset.

B. Experimental Setup

To implement the testing procedure explained in Section III-A, a battery test, thermal test equipment, and a PC are required. A simplified block diagram of all the required devices is reported in Fig. 1 using different colors

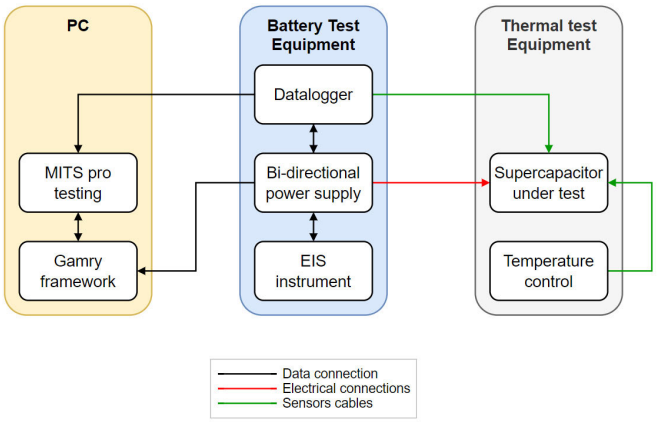

Fig. 1. Schematic representation of the entire experimental setup for characterization of HSC under different temperature and SOC conditions.

to represent the data connections (through USB or Ethernet cables), the electrical connections, and the sensor cables.

More in detail, the thermal test equipment is essentially made by LabEvent *LC*/150/40/5 climatic chamber by Weiss Technik characterized by a temperature regulation between −40 °C and 180 °C. A data logging unit is embedded within the chamber, and it can be used to ensure that the temperature required by the test plan is the actual temperature of the SC (and not the temperature of the surrounding environment). To do so, the control system of the climatic chamber uses an external control RTD placed in direct contact with the SC under test. The sensor is a class AA calibrated PT100 RTD characterized by a tolerance value of $\pm(0.1 + 0.0017|T|)$. Furthermore, other three PT100 sensors have been used to ensure that the temperature stability of the SC and surrounding ambient have been reached before actually starting the EIS measurements.

Furthermore, the other three RTDs are used to acquire the ambient temperature around the cell. However, these data are not used by the climatic chamber's controller.

The second main element of the experimental setup is the battery test equipment. It is composed of the following.

1) The Laboratory Battery Test System (LBT 5 V-30 A) by Arbin Instruments. It is a bidirectional power supply that can be used to charge and discharge up to 16 channels simultaneously, with a maximum voltage of 5 V and a maximum current per channel of 30 A. The system has a 24-bit resolution and a 100-ppm precision.
2) A Gamry Interface 5000E system for EIS measurements. This instrument can perform EIS in the 10 μHz ÷ 100 kHz frequency range when integrated with the Arbin battery tester.
3) An external and independent data-logging unit is used only for safety purposes to ensure that a test is interrupted if the temperature of the cell goes outside safety thresholds. The data logger uses two T-type thermocouples connected to the far ends of the SC.

The complete setup is shown in Fig. 2 and it also includes a PC with adequate software for the management of both the battery tester and EIS instrument.

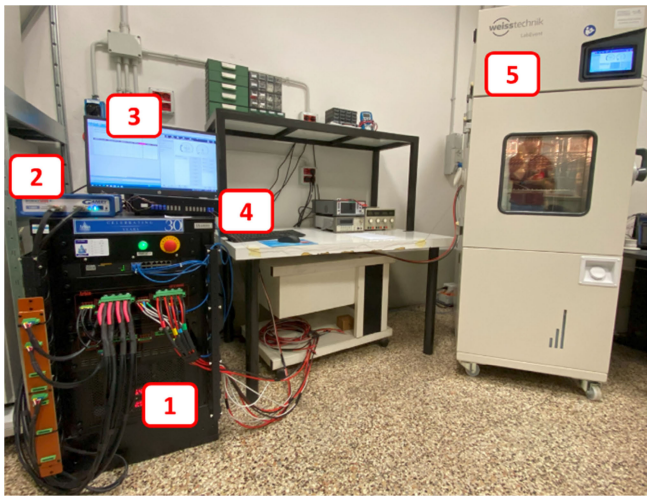

Fig. 2. Picture of the complete experimental setup. 1: bidirectional power supply. 2: EIS instrument. 3: PC with adequate software. 4: datalogger. 5: climatic chamber.

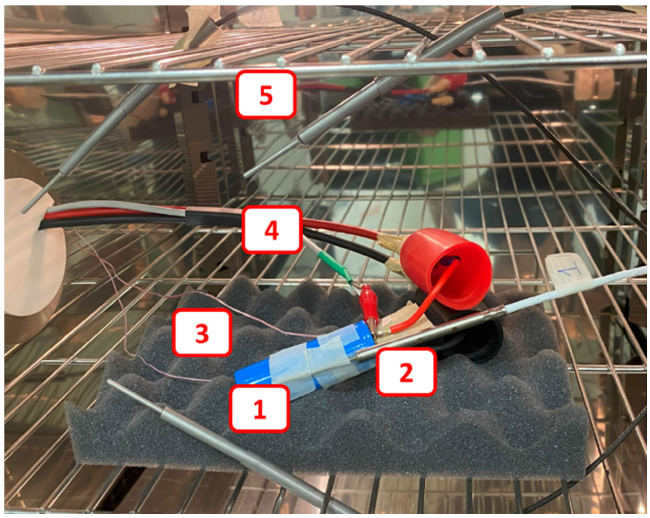

Fig. 3. Detail of the setup inside the climatic chamber showing—1: SC under test, 2: control PT100, 3: safety thermocouples, 4: electric connections; and 5: additional temperature sensors.

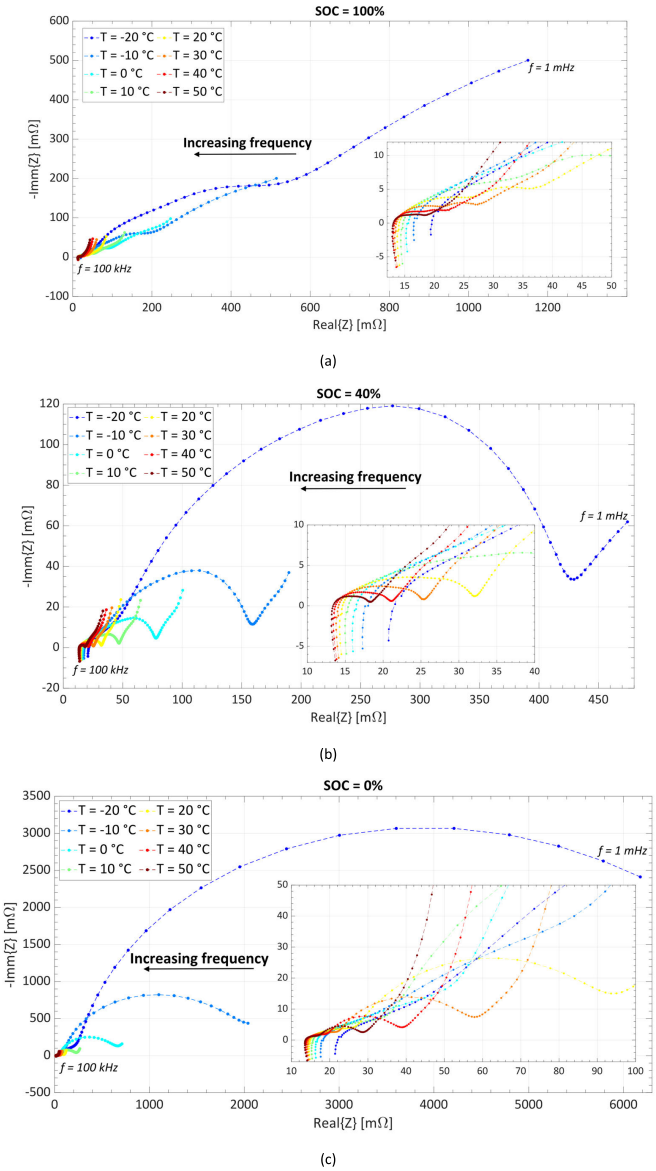

Fig. 4. Impedance spectroscopy at different temperatures. (a) Analysis with SOC = 100%. (b) Analysis with SOC = 40%. (c) Analysis with SOC = 0%.

The HSC located inside the chamber is connected to the battery tester using two current cables (power line) and two voltage cables (sense). The EIS instrument is connected to the battery tester, and it uses the abovementioned cables to excite the cell and measure its response. A detail of the device inside the chamber is reported in Fig. 3.

IV. Results and Discussion

This section reports a comparative analysis of the HSC impedance at different temperature conditions and different SOC values. More in detail, Fig. 4 compares the results of the EIS at different temperature values of the HSC with a fixed SOC condition. Three values of SOC are shown to highlight how the impedance is significantly changed depending on the operating conditions. More in detail, the impedance values obtained for different temperatures considering SOC = 0%, SOC = 40%, and SOC = 100% are compared in Fig. 4(a)–(c), respectively. The arrows in the graphs indicate the frequency information emphasizing the impedance variation when the frequency increases, while the different colors stand for different temperature conditions. For the sake of clarity, cold temperatures are illustrated in shades of blue, while orange and red trends stand for hot temperatures.

First, it can be noted that the greatest impedance variations occur at low temperatures, while at high temperatures, the impedance of the HSC is less variable. Independently of the SOC and the temperature, the HSC has a capacitive behavior at low frequencies, but it becomes inductive at high frequencies. When the SOC is low, a higher magnitude of impedance occurs, as can be seen by comparing the impedance curve for a specific temperature in Fig. 4(a) and (c). This is because, when the SOC of the HSC is low, there may be a greater presence of adsorbed ions on the electrode surface. This adsorption leads to a decrement in ion species within the HSC, such as ions available for charge conduction [45].

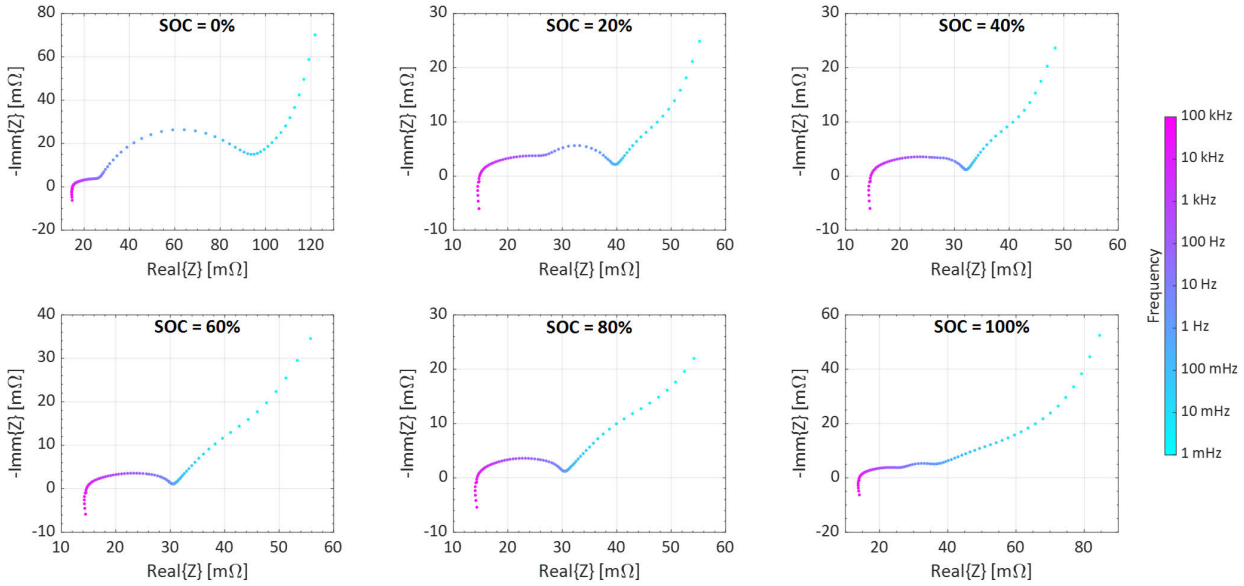

Fig. 5. Results of the impedance spectroscopy measurements at $T = 20$ °C for all the different analyzed SOCs. The colormap emphasizes the frequency of investigation.

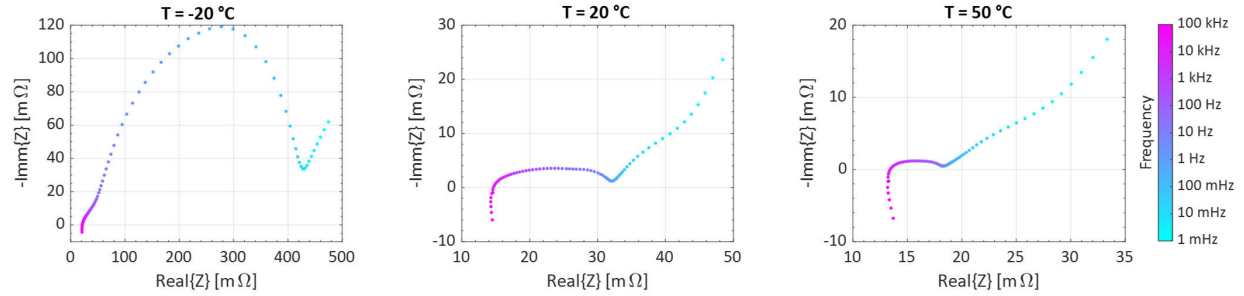

Fig. 6. Results of the impedance spectroscopy measurements performed at SOC = 40% for three different temperatures (minimum value, standard conditions, and maximum value).

This can influence the electrical response of the device and contribute to higher impedance values.

Another observation is that, at lower SOC, more Warburg curves occur. At low SOC, when the available electric charge in the HSC is reduced, ion diffusion can become slower. Warburg's parabolas are typically associated with diffusion processes, and, at low frequencies, they can reflect the ion diffusion response within the electrolyte or across the electrode/electrolyte interface layers.

When the SOC of the HSC is relatively low, the diffusion effect can be more pronounced, leading to the observation of multiple Warburg parabolas, as shown in Fig. 4(b) and (c).

SCs are known to have low internal resistance compared to other energy storage devices. At high SOC, the internal resistance of the HSC can be further reduced, contributing to the linearization of the spectroscopy curve at low frequencies, as shown in Fig. 4(a). This behavior is widely assumed in the literature. Anyway, what stands out from this comparative study is that for HSC, this assumption is valid only in the case of high SOC. For low SOC, the impedance is no longer linear, but the effects described above make the curve strongly parabolic, as shown in Fig. 4(c).

This last behavior can also be seen in Fig. 5, where the impedance at 20 °C and for all the different SOCs under investigation is shown. Instead, the effects of the temperature variations are shown in Fig. 6, where the EIS measured data point for an HSC with SOC = 40% for three different temperatures (i.e., minimum temperature, standard operating condition, and maximum temperature) are shown.

Note that Figs. 5 and 6 use a colormap codification to identify the different frequencies of investigation of the impedance during the EIS measurement, where the light blue points on the right side of the graphs stand for low frequencies, while the purple and fuchsia points stand for high frequencies. This type of graph allows us to appreciate the wide range of investigations and to rapidly understand the frequency value of the different data points.

The most striking result to emerge from Fig. 6 is that the impedance significantly increases at low temperatures (up to ten times). This behavior can be expected for this technology because, at lower temperatures, the mobility of ions within the electrolyte decreases. This can affect the speed of ion diffusion and, consequently, the impedance of the HSC. Reduced ionic mobility can cause an increase

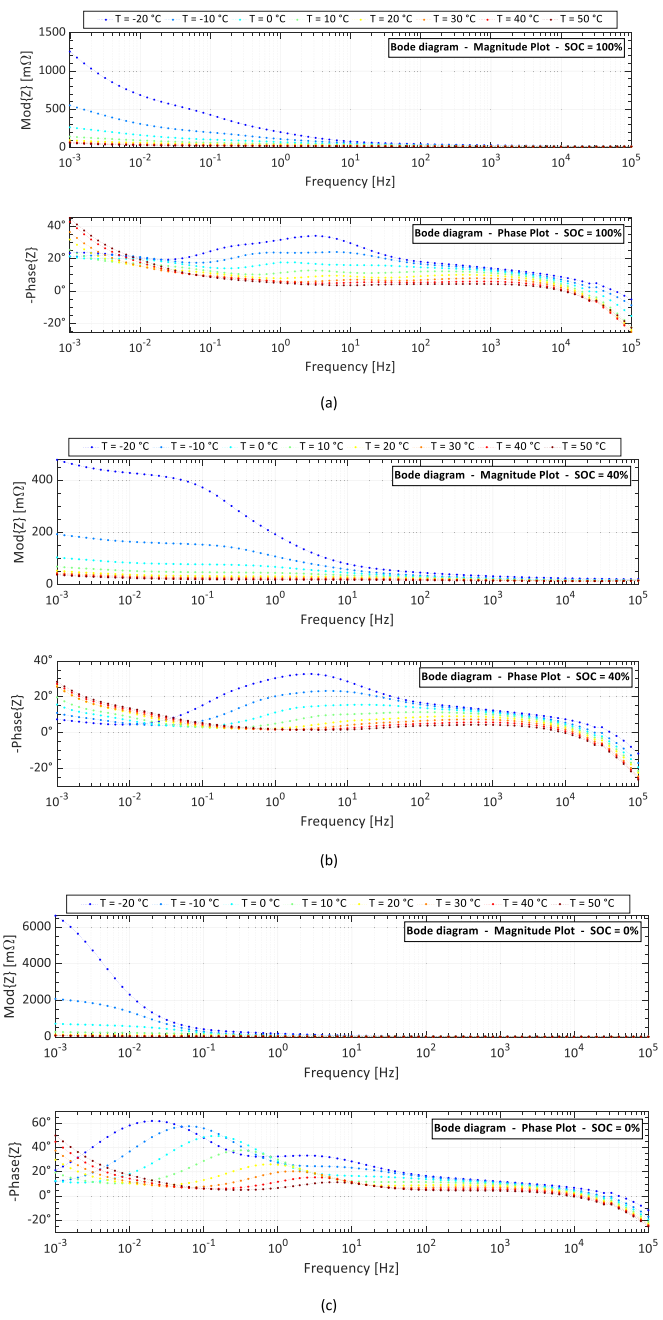

Fig. 7. Bode diagram of the impedance at different temperatures. (a) With SOC = 100%. (b) With SOC = 40%. (c) With SOC = 0%.

in electrical resistance and, consequently, in the measured impedance.

This effect can also be highlighted by the Bode plot shown in Fig. 7, where the impedance at three different SOCs is shown.

The effect is visible in Fig. 7 where, at low temperatures, i.e., at $T = -20$ °C (blue trend), the phase is significantly reduced, e.g., close to 0°, and the magnitude of the impedance increases.

Another interesting analysis is shown in the top subplot of Fig. 8, where the frequency at which the transition from a capacitive to an inductive behavior is reported as a function of temperature (x-axis) and SOCs (using a color code, where

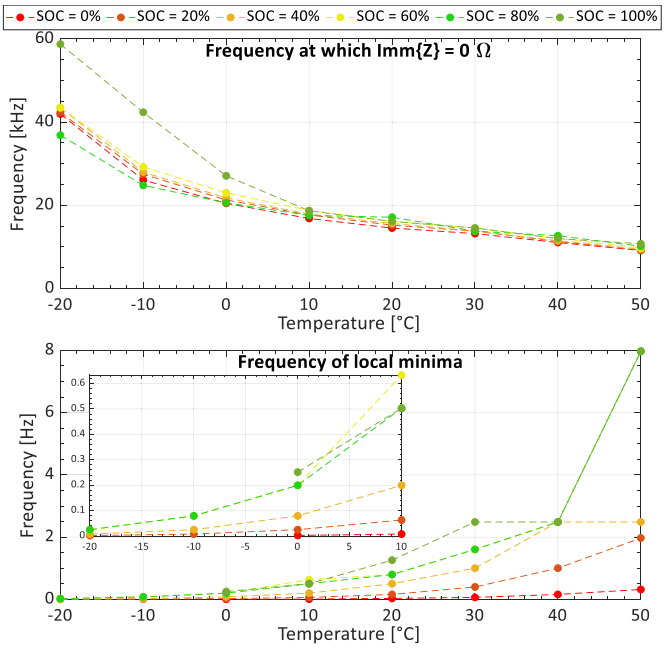

Fig. 8. Analysis of transition frequencies at different SOC and temperatures. Transition frequency from capacitive to inductive impedance is shown in the top subplot, while the bottom one refers to the frequency at which the local minima occur on the Warburg curve.

red is assigned to SOC = 0%, i.e., fully discharged cell, intermediate SOCs values are represented with orange and yellow, while a fully charged cell, i.e., SOC = 100%, is illustrated using green). The analyzed frequency decreases for higher temperatures because of the temperature influences on the rate of ion diffusion within the electrolyte.

At higher temperatures, ionic mobility increases, allowing for faster ion transport and a more rapid electrical response. This can result in a lower transition frequency from a capacitive behavior to an inductive behavior.

An opposite trend is instead illustrated in the bottom subplot of Fig. 8, where the frequency of the local minima on the Warburg curve is reported as a function of temperature (x-axis) and SOCs. In this case, the transition frequency increases when temperature increases, with the highest values obtained for the greatest SOC conditions. Furthermore, as can be seen in the zoom reported in Fig. 8, it is important to point out that the local minima are not even present when the temperature is extremely low (i.e., $T = -20$ °C or $T = -10$ °C) and the SOC conditions are 0% and 100%, emphasizing great changes in the impedance spectra at harsh conditions, such as extremely cold temperature, fully charged HSC, and fully discharged HSC.

Finally, in Fig. 9, the module of the impedance measured at three specific frequency values (i.e., $f = 1$ mHz, $f = 1$ Hz, and $f = 1$ kHz) is shown for different temperatures. As can be seen from the graphs, the module is substantially independent of the SOC when the EIS is performed at $f = 1$ kHz, which is the standard value reported by all manufacturers. However, when operating at low temperature and performing EIS at low frequency, it is possible to highlight significant variation according to the different SOC conditions. Anyway, performing low-frequency spectroscopy takes a long time,

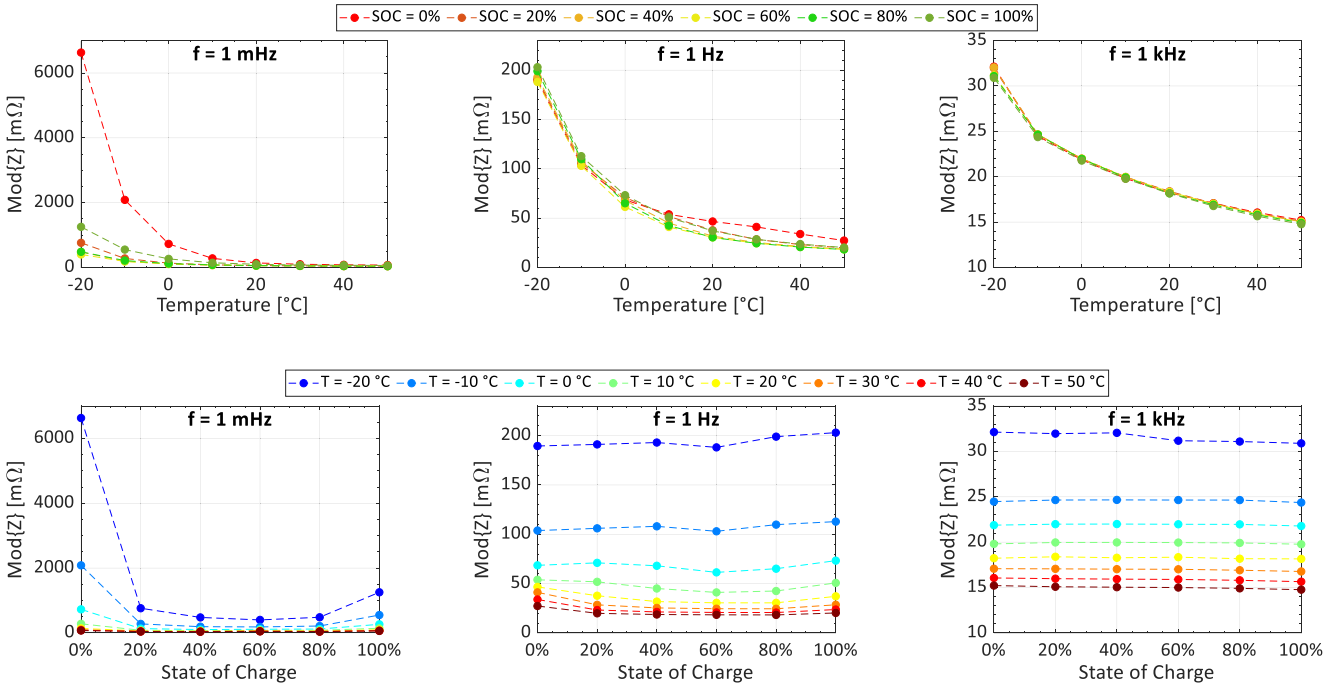

Fig. 9. Analysis of impedance variation at three fixed frequencies: $f = 1$ mHz on the left, $f = 1$ Hz on the center, and $f = 1$ kHz on the right.

which represents a critical aspect in many real-case applications. Thus, the analysis of the magnitude of the impedance is not particularly useful for estimating the SOC but can be used to estimate online the HSC cell temperature. A final consideration of Fig. 9 can be drawn regarding the actual impedance value measured at $f = 1$ kHz. According to the manufacturer, this value should be lower than 15 mΩ. Instead, values close to 15 mΩ have been obtained only at high-temperature conditions, while impedance rapidly increases when temperature decreases, reaching even a double value for negative temperature conditions.

V. Conclusion

In this work, an experimental characterization of a novel HSC by employing EIS measurement has been proposed.

The innovative contributions and the most salient outcome of this research can be summarized as follows.

1) At the moment, HSCs still represent an emerging and not deeply investigated energy storage technology. For this reason, an experimental characterization under different operating conditions of HSCs has been proposed.
2) A specific test plan and an experimental setup have been proposed to characterize the cell's performances by employing EIS measurement, considering a large frequency range (1 mHz ÷ 100 kHz) with ten data points per decade, six different operating conditions in terms of SOC (0%, 20%, 40%, 60%, 80%, 100%), and eight different operating temperatures in the range from −20 °C to 50 °C.
3) The changes in HSC impedance under harsh operating conditions have been studied and compared in this work for different SOC values. Such information is of primary importance because it can be used for multiple purposes, from correct SOC and state-of-health estimation to diagnostic of malfunctions and hazardous conditions.
4) The comparative analysis also allowed us to understand the operating limits in terms of working temperature. For example, from the results obtained, it is evident that when the cell operates at low temperatures, the internal resistance increases significantly leading to a strong degradation of the charge/discharge efficiency as the ohmic losses increase.

Future development will involve the use of the constructed dataset to develop the equivalent electric circuit of the cell as a function of the different operating conditions that have been studied.

Data Availability

The dataset used in this study is available at https://doi.org/10.6084/m9.figshare.24321496.

References

[1] M. R. Kumar, S. Ghosh, and S. Das, "Analytical formulation for power, energy, and efficiency measurement of ultracapacitor using fractional calculus," *IEEE Trans. Instrum. Meas.*, vol. 68, no. 12, pp. 4834–4844, Dec. 2019, doi: 10.1109/TIM.2019.2899479.

[2] Q. Deng, D. Qiu, Z. Xie, B. Zhang, and Y. Chen, "Online SOC estimation of supercapacitor energy storage system based on fractional-order model," *IEEE Trans. Instrum. Meas.*, vol. 72, pp. 1–10, 2023, doi: 10.1109/TIM.2023.3280524.

[3] M. Catelani, L. Ciani, R. Fantacci, G. Patrizi, and B. Picano, "Remaining useful life estimation for prognostics of lithium-ion batteries based on recurrent neural network," *IEEE Trans. Instrum. Meas.*, vol. 70, pp. 1–11, 2021, doi: 10.1109/TIM.2021.3111009.

[4] J. Yu, "State-of-Health monitoring and prediction of lithium-ion battery using probabilistic indication and state-space model," *IEEE Trans. Instrum. Meas.*, vol. 64, no. 11, pp. 2937–2949, Nov. 2015, doi: 10.1109/TIM.2015.2444237.

[5] B. Radej and G. Begeš, "An enhanced model for reliability prediction of a supercapacitor's lifetime: Developing an improved reliability model," *IEEE Ind. Electron. Mag.*, vol. 13, no. 3, pp. 26–34, Sep. 2019, doi: 10.1109/MIE.2019.2922417.

[6] G. Dotelli, R. Ferrero, P. Gallo Stampino, S. Latorrata, and S. Toscani, "Supercapacitor sizing for fast power dips in a hybrid supercapacitor—PEM fuel cell system," *IEEE Trans. Instrum. Meas.*, vol. 65, no. 10, pp. 2196–2203, Oct. 2016, doi: 10.1109/TIM.2016.2549658.

[7] F. Naseri, E. Farjah, Z. Kazemi, E. Schaltz, T. Ghanbari, and J.-L. Schanen, "Dynamic stabilization of DC traction systems using a supercapacitor-based active stabilizer with model predictive control," *IEEE Trans. Transport. Electrific.*, vol. 6, no. 1, pp. 228–240, Mar. 2020, doi: 10.1109/TTE.2020.2964423.

[8] S. Sahoo and P. Timmann, "Energy storage technologies for modern power systems: A detailed analysis of functionalities, potentials, and impacts," *IEEE Access*, vol. 11, pp. 49689–49729, 2023, doi: 10.1109/ACCESS.2023.3274504.

[9] X. Wang, Y. Luo, B. Qin, and L. Guo, "Power allocation strategy for urban rail HESS based on deep reinforcement learning sequential decision optimization," *IEEE Trans. Transport. Electrific.*, vol. 9, no. 2, pp. 2693–2710, Jun. 2023, doi: 10.1109/TTE.2022.3227900.

[10] J.-E. Baek, J.-H. Rhee, Y.-M. Cho, and K.-C. Ko, "A 25-F electric double-layer capacitor bank and DC power supply for portable high-current applications," *IEEE Trans. Plasma Sci.*, vol. 45, no. 8, pp. 2335–2340, Aug. 2017, doi: 10.1109/TPS.2017.2720782.

[11] R. Kunwar et al., "Characterization of electrochemical double layer capacitor electrode using self-discharge measurements and modeling," *Appl. Energy*, vol. 334, Mar. 2023, Art. no. 120658, doi: 10.1016/j.apenergy.2023.120658.

[12] F. Corti et al., "Time-domain circuit modelling for hybrid supercapacitors," *Energies*, vol. 14, no. 20, p. 6837, Oct. 2021, doi: 10.3390/en14206837.

[13] *Datasheet: 3.0V 3400F Ultracapacitor Cell Datasheet*, Maxwell Technologies, document 3002330-EN.2, 2018.

[14] J. Lee, "Shelf life of supercapacitor products," Electron. Division (Eaton), Pleasanton, CA, USA, Tech. Rep., Dec. 2016.

[15] S. Mahala, K. Khosravinia, and A. Kiani, "Unwanted degradation in pseudocapacitors: Challenges and opportunities," *J. Energy Storage*, vol. 67, Sep. 2023, Art. no. 107558, doi: 10.1016/j.est.2023.107558.

[16] P. Bhojane, "Recent advances and fundamentals of pseudocapacitors: Materials, mechanism, and its understanding," *J. Energy Storage*, vol. 45, Jan. 2022, Art. no. 103654, doi: 10.1016/j.est.2021.103654.

[17] J. Wang et al., "Pseudocapacitive materials for electrochemical capacitors: From rational synthesis to capacitance optimization," *Nat. Sci. Rev.*, vol. 4, no. 1, pp. 71–90, Jan. 2017, doi: 10.1093/nsr/nww072.

[18] A. Muzaffar, M. B. Ahamed, K. Deshmukh, and J. Thirumalai, "A review on recent advances in hybrid supercapacitors: Design, fabrication and applications," *Renew. Sustain. Energy Rev.*, vol. 101, pp. 123–145, Mar. 2019, doi: 10.1016/j.rser.2018.10.026.

[19] W. Liu et al., "Thermal characteristic and performance influence of a hybrid supercapacitor," *J. Energy Storage*, vol. 53, Sep. 2022, Art. no. 105188, doi: 10.1016/j.est.2022.105188.

[20] A. De Angelis, E. Buchicchio, F. Santoni, A. Moschitta, and P. Carbone, "Uncertainty characterization of a practical system for broadband measurement of battery EIS," *IEEE Trans. Instrum. Meas.*, vol. 71, pp. 1–9, 2022, doi: 10.1109/TIM.2022.3156994.

[21] C. Chang, S. Wang, C. Tao, J. Jiang, Y. Jiang, and L. Wang, "An improvement of equivalent circuit model for state of health estimation of lithium-ion batteries based on mid-frequency and low-frequency electrochemical impedance spectroscopy," *Measurement*, vol. 202, Oct. 2022, Art. no. 111795, doi: 10.1016/j.measurement.2022.111795.

[22] W. Zhang, T. Li, W. Wu, N. Ouyang, and G. Huang, "Data-driven state of health estimation in retired battery based on low and medium-frequency electrochemical impedance spectroscopy," *Measurement*, vol. 211, Apr. 2023, Art. no. 112597, doi: 10.1016/j.measurement.2023.112597.

[23] Z. Zhou, Y. Li, Q.-G. Wang, and J. Yu, "Health indicators identification of lithium-ion battery from electrochemical impedance spectroscopy using geometric analysis," *IEEE Trans. Instrum. Meas.*, vol. 72, pp. 1–9, 2023, doi: 10.1109/TIM.2023.3272401.

[24] M. Crescentini et al., "Online EIS and diagnostics on lithium-ion batteries by means of low-power integrated sensing and parametric modeling," *IEEE Trans. Instrum. Meas.*, vol. 70, pp. 1–11, 2021, doi: 10.1109/TIM.2020.3031185.

[25] G. Dotelli, R. Ferrero, P. G. Stampino, and S. Latorrata, "Analysis and compensation of PEM fuel cell instabilities in low-frequency EIS measurements," *IEEE Trans. Instrum. Meas.*, vol. 63, no. 7, pp. 1693–1700, Jul. 2014, doi: 10.1109/TIM.2013.2297632.

[26] P. A. Lindahl, M. A. Cornachione, and S. R. Shaw, "A time-domain least squares approach to electrochemical impedance spectroscopy," *IEEE Trans. Instrum. Meas.*, vol. 61, no. 12, pp. 3303–3311, Dec. 2012, doi: 10.1109/TIM.2012.2210457.

[27] N. T. Kemp, "A tutorial on electrochemical impedance spectroscopy and nanogap electrodes for biosensing applications," *IEEE Sensors J.*, vol. 21, no. 20, pp. 22232–22245, Oct. 2021, doi: 10.1109/JSEN.2021.3084284.

[28] S. Buller, E. Karden, D. Kok, and R. W. De Doncker, "Modeling the dynamic behavior of supercapacitors using impedance spectroscopy," *IEEE Trans. Ind. Appl.*, vol. 38, no. 6, pp. 1622–1626, Nov. 2002, doi: 10.1109/TIA.2002.804762.

[29] R. Kötz, M. Hahn, and R. Gallay, "Temperature behavior and impedance fundamentals of supercapacitors," *J. Power Sources*, vol. 154, no. 2, pp. 550–555, Mar. 2006, doi: 10.1016/j.jpowsour.2005.10.048.

[30] L. Zhang, Z. Wang, X. Hu, and D. G. Dorrell, "Experimental investigation of ultracapacitor impedance characteristics," *Energy Proc.*, vol. 75, pp. 1888–1894, Aug. 2015, doi: 10.1016/j.egypro.2015.07.173.

[31] G. Xiong, A. Kundu, and T. S. Fisher, "Influence of temperature on supercapacitor performance," in *Thermal Effects in Supercapacitors* (Briefs in Applied Sciences and Technology). USA; Springer, 2015, pp. 71–114, doi: 10.1007/978-3-319-20242-6_4.

[32] S. Buller, M. Thele, R. W. A. A. Dedoncker, and E. Karden, "Impedance-based simulation models of supercapacitors and Li-ion batteries for power electronic applications," *IEEE Trans. Ind. Appl.*, vol. 41, no. 3, pp. 742–747, May 2005, doi: 10.1109/TIA.2005.847280.

[33] M. Marracci, B. Tellini, M. Catelani, and L. Ciani, "Ultracapacitor degradation state diagnosis via electrochemical impedance spectroscopy," *IEEE Trans. Instrum. Meas.*, vol. 64, no. 7, pp. 1916–1921, Jul. 2015, doi: 10.1109/TIM.2014.2367772.

[34] A. El Mejdoubi, A. Oukaour, H. Chaoui, Y. Slamani, J. Sabor, and H. Gualous, "Online supercapacitor diagnosis for electric vehicle applications," *IEEE Trans. Veh. Technol.*, vol. 65, no. 6, pp. 4241–4252, Jun. 2016, doi: 10.1109/TVT.2015.2454520.

[35] H. Ahmad, W. Y. Wan, and D. Isa, "Modeling the ageing effect of cycling using a supercapacitor-module under high temperature with electrochemical impedance spectroscopy test," *IEEE Trans. Rel.*, vol. 68, no. 1, pp. 109–121, Mar. 2019, doi: 10.1109/TR.2018.2869212.

[36] A. El Mejdoubi, H. Chaoui, H. Gualous, and J. Sabor, "Online parameter identification for supercapacitor state-of-health diagnosis for vehicular applications," *IEEE Trans. Power Electron.*, vol. 32, no. 12, pp. 9355–9363, Dec. 2017, doi: 10.1109/TPEL.2017.2655578.

[37] S. Moayedi, F. Cingöz, and A. Davoudi, "Accelerated simulation of high-fidelity models of supercapacitors using waveform relaxation techniques," *IEEE Trans. Power Electron.*, vol. 28, no. 11, pp. 4903–4909, Nov. 2013, doi: 10.1109/TPEL.2013.2250522.

[38] A. Hammar, P. Venet, R. Lallemand, G. Coquery, and G. Rojat, "Study of accelerated aging of supercapacitors for transport applications," *IEEE Trans. Ind. Electron.*, vol. 57, no. 12, pp. 3972–3979, Dec. 2010, doi: 10.1109/TIE.2010.2048832.

[39] E. H. El Brouji, O. Briat, J.-M. Vinassa, N. Bertrand, and E. Woirgard, "Impact of calendar life and cycling ageing on supercapacitor performance," *IEEE Trans. Veh. Technol.*, vol. 58, no. 8, pp. 3917–3929, Oct. 2009, doi: 10.1109/TVT.2009.2028431.

[40] V. Mali and B. Tripathi, "Thermal stability of supercapacitor for hybrid energy storage system in lightweight electric vehicles: Simulation and experiments," *J. Modern Power Syst. Clean Energy*, vol. 10, no. 1, pp. 170–178, Jan. 2022, doi: 10.35833/MPCE.2020.000311.

[41] C. T. Sarr, M. B. Camara, and B. Dakyo, "Supercapacitors characterization using impedance spectroscopy and taking account dynamics contraints and their combinations," in *Proc. 8th Int. Conf. Renew. Energy Res. Appl. (ICRERA)*, Nov. 2019, pp. 359–364, doi: 10.1109/ICRERA47325.2019.8997005.

[42] W. Lajnef, J.-M. Vinassa, O. Briat, S. Azzopardi, and C. Zardini, "Study of ultracapacitors dynamic behaviour using impedance frequency analysis on a specific test bench," in *Proc. IEEE Int. Symp. Ind. Electron.*, 2004, pp. 839–844, doi: 10.1109/ISIE.2004.1571922.

[43] *Product Specification: 4.2 V 4000F GongHe04R2D24690SP*, GongHe Electronics, Rev. A2.0., Dongguan, China, 2022.

[44] X. Zhang et al., "Partially reduced graphene oxide-based electrolyte: Synthesis and electrochemical capacitance performance," *J. Mater. Sci.*, vol. 57, no. 22, pp. 10271–10284, Jun. 2022, doi: 10.1007/s10853-022-07298-2.

[45] S. Srivastav, M. Kumar, and R. Kant, "Theory for influence of uncompensated solution resistance on EIS of diffusion limited adsorption at rough electrode," *J. Chem. Sci.*, vol. 133, no. 2, p. 50, Jun. 2021, doi: 10.1007/s12039-021-01901-w.

Marcantonio Catelani (Member, IEEE) received the M.S. degree in electronic engineering from the University of Florence, Florence, Italy, in 1984.

He is currently with the Department of Information Engineering, University of Florence. Strictly correlated with reliability, availability, maintainability, and safety (RAMS) are the fields of interest of both fault diagnosis and reliability testing for components and equipment. In particular, the research activity concerns the development of test profiles used both for the characterization and the evaluation of reliability performance and, at the same time, the development of new degradation models able to estimate the life cycle of electronic components. His current research interests include the development of automatic measurement system, the characterization of A/D converters, quality control and related statistical methods, and RAMS context.

Lorenzo Ciani (Senior Member, IEEE) received the M.S. degree in electronic engineering and the Ph.D. degree in industrial and reliability engineering from the University of Florence, Florence, Italy, in 2005 and 2009, respectively.

He is currently an Associate Professor with the Department of Information Engineering, University of Florence. He has authored or coauthored more than 200 peer-reviewed journal and conference papers. His current research interests include system reliability, availability, maintainability and safety, reliability evaluation test and analysis for electronic systems and devices, fault detection and diagnosis, and electrical and electronic instrumentation and measurement.

Dr. Ciani is a member of the IEEE IMS TC-32 Fault Tolerant Measurement Systems. He is an Associate Editor-in-Chief of IEEE TRANSACTION ON INSTRUMENTATION AND MEASUREMENT and an Associate Editor of IEEE ACCESS. He received the 2015 IEEE I&M Outstanding Young Engineer Award for "his contribution to the advancement of instrumentation and measurement in the field of reliability analysis."

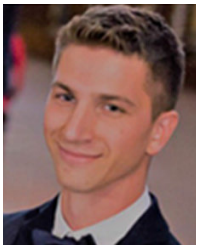

Fabio Corti (Member, IEEE) received the M.S. degree in electrical and automation engineering and the Ph.D. degree in industrial engineering from the University of Florence, Florence, Italy, in 2016 and 2019, respectively.

He was a Post-Doctoral Research Fellow with Consiglio Nazionale delle Ricerche, Florence, in 2020. From 2020 to 2022, he was a Post-Doctoral Research Fellow with the University of Perugia, Perugia, Italy. He is currently an Assistant Professor with the University of Florence. His research interests include modeling and control of dc–dc PWM and resonant converters, wireless power transfer, energy storage characterization, and electric vehicle powertrain.

Maurizio Laschi received the B.S. degree in mechanical engineering and the M.S. degree in energetic engineering from the University of Florence, Florence, Italy, in 2016 and 2021, respectively, where he is currently pursuing the Ph.D. degree in design and development of industrial products and processes.

His research activities are concentrated in the fields of energy storage for power units used in vehicles for micromobility.

Gabriele Patrizi (Member, IEEE) received the master's degree (cum laude) in electronic engineering and the Ph.D. degree in industrial and reliability engineering from the University of Florence, Florence, Italy, in 2018 and 2022, respectively.

In 2022, he joined the Institute of Electronic Packaging Technology (IAVT), Dresden Technical University, Dresden, Germany, as a Visiting Post-Doctoral Researcher. He is currently a Post-Doctoral Research Fellow in the field of instrumentation and measurement and an Adjunct Lecturer of electric measurements with the University of Florence. His research interests include life cycle reliability, condition monitoring for fault diagnosis of electronics, data-driven prognostic and health management, and instrumentation and measurement for reliability analysis.

Dr. Patrizi was a recipient of the "2023 Best Dissertation Award" from the IEEE IMS. He has been an Associate Editor of IEEE TRANSACTIONS ON INSTRUMENTATION AND MEASUREMENT (TIM) since 2023.

Alberto Reatti (Member, IEEE) received the M.S. degree in electronics engineering from the University of Florence, Italy, in 1988, and the Ph.D. degree from the University of Bologna, Bologna, Italy, in 1993.

In 1992, he was an Associate Researcher with the Department of Electrical Engineering, Wright State University, Dayton, OH, USA. He has been an Associate Professor with the Department of Information Engineering, University of Florence, since 2000. He is responsible for agreements of cultural and scientific cooperation at the Department of Information Engineering and the Head of the Patent and Technology Transfer Board, University of Florence. He has authored or coauthored more than 110 papers. He holds two patents. His current research interests include high-frequency, resonant, and pulsewidth modulated dc–dc power converters; dc–ac inverters; modeling and control of converters; high-frequency magnetic devices; renewable power sources; energy saving; wireless power transfer; and investigations on reliability of switching power converters.

Dr. Reatti has served as the Chairperson for the Power Electronic and Power Systems Committee of the IEEE CAS Society.

Dario Vangi received the master's degree in mechanical engineering and the Ph.D. degree in quality engineering from the University of Florence, Florence, Italy, in 1988 and 1992, respectively.

He is currently an Associate Professor with the Department of Industrial Engineering, University of Florence. Additionally, he maintains membership with the IGLAD-Initiative for the global harmonization of accident data, the World Road Association-PIARC, and EVU-European road accident analysis. His research interests consist of road accident analysis and reconstruction, examination of sustainable mobility applications, and nondestructive evaluation.

Open Access funding provided by 'Università degli Studi di Firenze' within the CRUI CARE Agreement